Journal of Hydrology: Regional Studies 5 (2016) 80–99

Contents lists available at ScienceDirect

Journal of Hydrology: Regional Studies

journal homepage: www.elsevier.com/locate/ejrh

The influence of climate modes on streamflow in the Mid-Atlantic region of the United States

Justin A. Schulte [a,*], Raymond G. Najjar [a], Ming Li [b]

[a] Department of Meteorology, The Pennsylvania State University, University Park, 503 Walker Building, PA 16802, USA
[b] Horn Point Laboratory, University of Maryland Center for Environmental Science, P.O. Box 775, Cambridge, MD 21613, USA

ARTICLE INFO

Article history:
Received 2 May 2015
Received in revised form 6 November 2015
Accepted 10 November 2015
Available online 12 December 2015

Keywords:
Streamflow
Climate
Climate variability
Wavelet analysis
El-Niño-Southern Oscillation
Mid-Atlantic region

ABSTRACT

Study region: The Mid-Atlantic region of the United States.
Study focus: An understanding of past streamflow variability is necessary for developing future management practices that will help mitigate the impacts of extreme events such as drought or floods on agriculture and other human activities. To better understand mechanisms driving streamflow variability at all timescales, annual to multi-decadal streamflow variability of three major rivers in the Mid-Atlantic region of the United States (the Susquehanna, Delaware, and Hudson Rivers) was studied in the context of climate modes using correlation and wavelet analyses.
New hydrological insights for the region: Results from the correlation analysis detected statistically significant relationships between climate indices and streamflow that were similar for the three rivers. The results from the wavelet analysis showed that 18- and 26-year periodicities were embedded in the streamflow time series. Decadal variability of streamflow was coherent with the El-Niño Southern Oscillation (SO) and the Pacific Decadal Oscillation (PDO). The time series for the PDO and SO indices and precipitation were found to be synchronized to the decadal variability of a global circulation pattern consisting of a Rossby wave train emanating from the North Pacific. The SO explained 37–54% of the 1960s drought, 33–49% of the 1970s pluvial, and 19–50% of the 2000s pluvial in the three river basins.

1. Introduction

The Susquehanna, Delaware, and Hudson River Basins (SRB, DRB, and HRB) drain to three important estuaries of the Mid-Atlantic region of the United States (US, Fig. 1), which have experienced substantial climate change and are likely to continue do so with increases in greenhouse gas concentrations (Najjar et al., 2009). This projected climate change is likely to render more difficult efforts to restore these estuaries, which have been stressed by anthropogenic activities, including pollution (e.g., toxic metals, polychlorinated biphenyls, and excess nitrogen), dredging, conversion of wetland habitats, and overfishing (Najjar et al., 2010; Kreeger et al., 2010; Steinberg et al., 2004).

Climate change is likely to manifest itself through changes in existing climate modes, which are recurring and often oscillatory patterns of climate variables, such as sea level pressure (SLP) and sea surface temperature (SST), that operate on timescales ranging from weekly to multi-decadal. For example, Ning et al. (2012) found increases in projected wintertime

* Corresponding author.
E-mail addresses: jas6367@psu.edu (J.A. Schulte), rgn1@psu.edu (R.G. Najjar), Mingli@umces.edu (M. Li).

http://dx.doi.org/10.1016/j.ejrh.2015.11.003

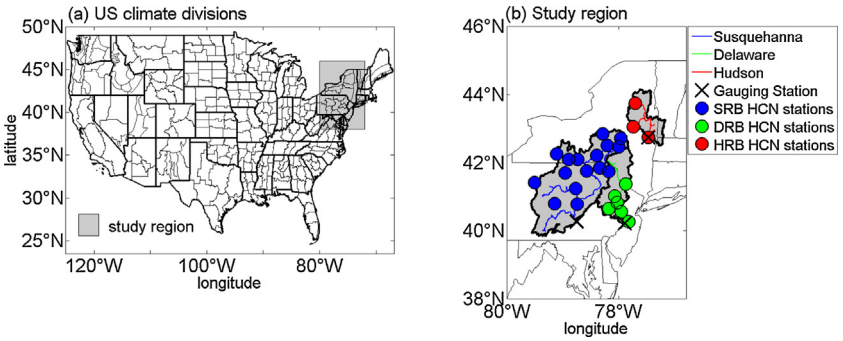

Fig. 1. (a) Location of the US climate divisions delimited with thin black lines. State boundaries are thick black lines and the study region is indicated by the gray box. (b) Locations of the Harrisburg gauging in the Susquehanna River Basin (SRB), the Trenton gauging station in the Delaware River Basin (DRB), and the Waterford gauging station in the Hudson River Basin (HRB) and Historical Climate Network stations. Thick black lines represent the boundaries of the Harrisburg, Trenton, and Waterford drainage basins and thin lines represent state boundaries.

precipitation in the Northeast US to be consistent with a projected decrease in the positive phase of one prominent climate mode, the North Atlantic Oscillation (NAO). The NAO and other important climate modes, such as the Atlantic Multi-decadal Oscillation (AMO), the Pacific Decadal Oscillation (PDO), El Niño-Southern Oscillation (ENSO), the Pacific Northern-American Teleconnection (PNA), and the North Pacific Oscillation (NPO), have regional- to global-scale impacts on climate and weather (Philander, 1983; Trenberth and Hurrell, 1994; Mantua et al., 1997; Thompson and Wallace, 1998; Hurrell et al., 2003).

An understanding of the historical impacts of climate modes on regional climate variability can enhance our understanding of future changes in that region. Furthermore, an understanding of climate-mode impacts on regional meteorological, hydrological, and ecological characteristics will improve monthly and seasonal forecasts, which are of economic importance. With that in mind, the goal of this study is to analyze the variability in streamflow of the Susquehanna, Delaware, and Hudson Rivers, three large rivers in the Mid-Atlantic region of the US, in the context of climate modes.

There are relatively few studies on the impacts of climate modes on streamflow variability in the Mid-Atlantic region as compared to precipitation-climate mode and temperature-climate mode studies. Dettinger and Diaz (2000) found associations between the December–February Southern Oscillation (SO) and October–September streamflow across the Northeast, where El Niño years are associated with wetter-than-normal conditions. Futhuremore, Xu et al. (2012) identified relationships between North Pacific SSTs and Northeast US streamflow and Barlow et al. (2001) found North Pacific SSTs to have been possible drivers of the 1960s drought, a major hydrometeorological event that strained water-management agreements between New York City and Philadelphia (USDA, 2000). The relationships may be the result of prevailing synoptic regimes that set up during certain NAO and ENSO phases (Miller et al., 2006). Barlow et al. (2001) and Miller et al. (2006), however, only considered climate mode-streamflow simultaneous relationships. It is not clear if relationships hold on decadal and multi-decadal timescales. Labat (2008) and Whitney (2010) investigated streamflow variability across the Mid-Atlantic Bight and found multi-decadal variability in the flows of many rivers in the region, which Whitney (2010) hypothesized was related to the NAO.

The streamflow-climate mode relationships discussed above are associated with changes in precipitation, temperature, snow cover, and evapotranspiration, all of which have been investigated in the context of climate modes. Leathers et al. (1991) found that positive PNA phases are accompanied by colder and drier conditions across the US on monthly timescales. Serreze et al. (1998) noted increased snowfall in the Mid-Atlantic region during positive phases of the PNA, which was found to be associated with below-normal maximum temperature on precipitation days. Barlow et al. (2001) noted ENSO, NPO, and PDO influences on Northeast US precipitation and drought conditions. Pattern et al. (2003) found associations between ENSO and winter snowfall across the Northeast US, with El Niño years being accompanied by more frequent major snow events. Archambault et al. (2008) found cool seasons under positive NAO and negative PNA regimes to be wettest. Eichler and Higgins (2006) found increased spring precipitation during El Niño years as a result of more frequent East Coast storms. Similarly, Seager et al. (2010) found strong winter snowfall-NAO and snowfall-ENSO linkages, both of which were related to the frequency of East Coast storms. Despite the impact of ENSO on Northeast precipitation, previous research did not relate ENSO to the 1960s drought in the Northeast US; in fact, it has been argued that the drought (and the subsequent wet period that continues to the present) resulted from internal atmospheric variability because global climate models with prescribed SSTs did not reproduce the drought (Seager et al., 2012).

This paper presents a comprehensive investigation into climate-mode impacts on Mid-Atlantic streamflow by considering all timescales ranging from months to decades. To understand the proximate forcing of Mid-Atlantic streamflow, data sets on mean watershed temperature and precipitation are analyzed as well. Relationships among streamflow, precipitation, temperature, and climate indices are investigated first through a standard linear correlation analysis at monthly, seasonal, and annual timescales. A more general understanding of the variability of Mid-Atlantic streamflow and its linkages to the proximate climate and climate modes is obtained via wavelet analysis and wavelet coherence analysis.

The main advantage of wavelet analysis is that it can decompose a complex time series, such as streamflow, into a two-dimensional (time and frequency) representation, from which inferences about the time series can be drawn. Wavelet analysis can, in particular, detect important features embedded in the time series, such as modes of dominant variability and their temporal behavior, which may be linked to some physical mechanisms, facilitating further scientific investigation. The previously noted studies by Labat (2008) and Whitney (2010) detected decadal streamflow variability but did not quantitatively link it to physical mechanisms, underscoring the need to evaluate the relationship between multi-decadal streamflow variability and large-scale climate indices.

The relationship between streamflow and a climate index at a variety of timescales can be quantified using wavelet coherence analysis, which has the advantage of minimizing aliasing while also eliminating the choice of averaging window or filter. Climate modes are typically most energetic at certain periods so that climate mode-streamflow relationships may be used to identify particular timescales. The PDO, as an example, is most energetic at periods of 15–25 years and 50–70 years and therefore one might expect its influence to be strongest at those timescales (Mantua and Hare, 2002).

Another advantage of wavelet coherence analysis is that phase relationships at a given timescale can be quantified as a function of time. The goal of a traditional cross-correlation analysis is to determine the time delay for which the association between two time series is greatest, but one cannot determine how the relationship changes over time. In a wavelet coherence analysis, on the other hand, phase relationships are calculated such that the degree to which two time series are positively or negatively related can be measured as both a function of time and period. Such a decomposition is important in this study because the temporal variations of ENSO teleconnections result from differences in the atmospheric basic state during ENSO events and are modulated by other teleconnection patterns (Gershunov and Barnett, 1998).

The remainder of the paper is organized as follows. Section 2 describes the data sets used (streamflow, temperature, precipitation, and climate indices) and the methods employed (correlation and wavelet analysis). Section 3 first provides a brief description of Mid-Atlantic streamflow and precipitation variability, and then presents the main results: the outcomes of the linear correlation and wavelet analyses. Section 3 also presents an analysis of climate-mode contributions to decadal-scale Mid-Atlantic streamflow anomalies. Section 4 provides a brief discussion of the possible teleconnection patterns that link climate modes to Mid-Atlantic hydrology and Section 5 summarizes the analysis with some concluding remarks.

2. Data and methods

2.1. Streamflow, temperature, and precipitation

Mean monthly streamflow data were obtained from the United States Geological Survey (USGS) for the Delaware, Hudson, and Susquehanna Rivers at the Trenton, Waterford, and Harrisburg gauging stations, respectively (Fig. 1a and b), which have corresponding USGS station numbers of 1463500, 1335754, and 1570500. These gauging stations were chosen because of their relatively large drainage areas and long records. The reason for using gauging stations with large drainage basins is that high-frequency weather fluctuations across the basins are integrated over a larger area, which can enhance climate signal detection. The period of record used in this study is 1900–2010 for the Susquehanna and Hudson Rivers, and 1913–2010 for the Delaware River. These records are complete except for the Hudson River at Waterford, which has a few missing months in 1976 (0.9% of the record). These gaps were filled by linearly regressing streamflow from the nearby Green Island gauging station (USGS station number 1358000) with Waterford streamflow from 1950 to 2010 (Pearson correlation coefficient equals 0.99). All streamflow data were converted to anomalies by subtracting the climatological mean monthly value for each month from the monthly values, thereby removing the annual cycle.

Mean monthly maximum temperature and mean monthly precipitation data for 1900–2010 were obtained from the Historical Climate Network (HCN; Menne et al., 2009); station locations are shown in Fig. 1. The reason for using maximum temperature data is that precipitation type in the Northeast US is impacted by mean maximum temperature on precipitation days (Serreze et al., 1998). Compared to other precipitation and temperature data sets, the HCN data are of relatively high quality and long record length, which facilitates analysis on long timescales. To emphasize the basin-wide impacts of climate modes, the station-based precipitation and temperature data were averaged without any weighting to obtain a time series for each of the three river basins upstream of the gauging station. Like streamflow, the precipitation and temperature time series were converted to anomalies.

A few stations used in the averaging are located just outside the drainage basins. These stations were included in order to improve the significance of the basin-wide averages. Although precipitation at these stations will not directly contribute to streamflow at the gauging station in question, the distances between the boundaries of the drainage basins and the stations are small so it is expected that even mesoscale convective precipitation events contributed to precipitation at the drainage basin boundaries and the stations similarly.

Monthly climate divisional data were also used to understand spatial variability in climate-mode precipitation relationships (Fig. 1a). The data, extending back to 1895, are available for 344 climate divisions, regions within states that have a uniform climatology, eight to ten for each state (Guttman and Quayle, 1996). In the present study, only the precipitation data for the period 1900–2010 were used and converted to anomalies like the previously mentioned data sets. The benefit of using the divisional data versus the station-based HCN data is that local climatological effects can be smoothed out, allowing better detection of climate signals.

Table 1
Climate indices, data sources, record lengths, and relevant publications.

Climate index	Source	Record length used	References
NAO	NCAR	1900–2010	Hurrell et al. (2003)
AO	CPC	1950–2010	Thompson and Wallace (1998)
AMO	CPC	1900–2010	Enfield et al. (2001), Trenberth and Shea (2005)
Nino 3.4	NCAR	1900–2010	Trenberth (1997)
SO	NCAR	1900–2010	Trenberth (1984)
NPO	NCAR	1900–2010	Trenberth and Hurrell (1994)
PNA	CPC	1950–2010	Wallace and Gutzler (1981)
PDO	UW	1900–2010	Mantua et al. (1997), Mantua and Hare (2002)

Twentieth century reanalysis (Compo et al., 2011) 500-hPa geopotential height data from 1900 to 2010 were used to put results in a climatic context. The data are on a $2^\circ \times 2^\circ$ global grid and are produced from the assimilation of meteorological data, including observed surface pressure and sea-level pressure data. The annual cycle was removed from the data at each grid point.

2.2. Climate indices

For this study, eight climate indices were selected (Table 1) based on studies that have identified physical relationships between climate modes and precipitation and streamflow in the Mid-Atlantic region (see Section 1). We first briefly describe the indices before discussing the sources of the data.

Perhaps the most well-known climate mode is ENSO, whose evolution and strength can be monitored using two metrics, the Southern Oscillation Index (SOI) and the Niño 3.4 index (Trenberth, 1984, 1997), which capture the atmospheric and oceanic components, respectively, of ENSO. The SOI is calculated as the difference of SLP anomalies between Tahiti and Darwin, Australia. The Niño 3.4 index is defined as the average SST in the region 5°N–5°S, 170°W–120°W.

The climate modes most closely linked to the North Pacific region are the NPO, PDO, and PNA. The North Pacific Index, which describes the NPO, is defined as the area-weighted SLP over the region 30°N–65°N, 160°E–140°W (Trenberth and Hurrell, 1994). The PDO index is constructed from the leading mode of an un-rotated Empirical Orthogonal Function (EOF) analysis of monthly residual SST anomalies in the North Pacific poleward of 20°N, where the monthly residual is the difference between the observed anomaly and the global-mean SST anomaly (Mantua et al., 1997; Mantua and Hare, 2002). The PNA index is constructed from a rotated EOF analysis of daily 500-hPa geopotential height anomalies in the region bounded by 20°N and 90°N in the Northern Hemisphere (Barnston and Livezey, 1987).

Metrics of climate variability related to the North Atlantic Ocean are the AMO and NAO indices. The Atlantic basin exhibits SST variability with a preferred multi-decadal timescale. This multi-decadal oscillation of SST has been termed the AMO (Kerr, 2000), whose index is defined as the detrended average SST in the North Atlantic basin from 0° to 70°N (Enfield et al., 2001; Trenberth and Shea, 2005). The NAO consists of a dipole SLP pattern established by the Azores High and the Icelandic Low and the NAO index is defined as the normalized SLP difference between these pressure centers (Hurrell et al., 2003). A climate mode related to the NAO is the AO, an oscillation of the polar vortex. The AO index is constructed by standardizing the first principle component time series of northern-hemisphere SLP for all months of the year (Thompson and Wallace, 1998).

Climate index data used in the analysis (Table 1) were obtained from the Climate Prediction Center (CPC), the National Center for Atmospheric Research (NCAR, http://www.cgd.ucar.edu/cas/catalog/climind/), and the University of Washington (UW, http://jisao.washington.edu/pdo/PDO.latest). All data are monthly averages and, when necessary, were converted to anomalies by removing the mean annual cycle. All of the indices were available for the period 1900–2010, except those for the AO and PNA, which were available for the period 1950–2010. For consistency, the correlation analysis was applied to all eight indices for the period 1950–2010. The wavelet analysis was applied to all indices, except those for the AO and PNA, for the period 1900–2010.

2.3. Correlation analysis

Linear Pearson correlation coefficients between streamflow and climate indices, between precipitation and climate indices, and between temperature and climate indices were computed using monthly, seasonal, and annual averages for the period 1950–2010. Means were identified as DJF (December, January, February) for winter, MAM (March, April, May) for spring, JJA (June, July, August) for summer, and SON (September, October, November) for fall. The water year (October–September) was used for the annual means. Seasonal averages were computed because many climate modes are preferentially expressed in certain seasons. For example, it is in the Northern Hemisphere winter that the NAO and the AO often reach their maximum amplitudes and have the strongest influence. Significance was tested using the non-parametric bootstrap method (Efron, 1979) as follows: the data were resampled 10,000 times, correlation coefficients from the resampled data were computed, and then 95% and 99% confidence intervals of the resulting distribution of synthetic correlation coefficients were computed. Correlation coefficients were rejected at the 5% significance level if the confidence interval contained a correlation coefficient of zero.

Correlation analysis was also used to quantify the impact of precipitation and temperature on streamflow. Linear Pearson correlation coefficients were computed for each calendar month between streamflow and precipitation for 1950–2010. Temperature can influence streamflow variability through evapotranspiration, snowfall, and snowmelt. In fact, in the New England region, the significant storage of water in snow results in temperature explaining up to 30% of streamflow variability (Bradbury et al., 2002). In the SRB, Najjar (1999) found that annual precipitation minus streamflow (a proxy for annual evapotranspiration) was positively correlated with temperature. Nevertheless, precipitation dominates the streamflow signal so that temperature-streamflow relationships may appear to be non-existent or weak. Therefore, the partial correlation coefficient (Mattson, 1981) between temperature (t) and streamflow (q), controlling for precipitation (p), was computed for each calendar month for 1950–2010, which allows temperature impacts on streamflow to be assessed with the precipitation-streamflow dependence removed:

$$r_{tq,p} = \frac{r_{tq} - r_{tp} \times r_{qp}}{\sqrt{\left(1 - r_{tp}^2\right)\left(1 - r_{qp}^2\right)}}, \tag{1}$$

where r_{xy} represents the simple correlation coefficient between x and y. The partial correlation coefficient can be equal to the simple correlation coefficient or it can be very different depending on how strong the influence of the third variable is on the relationship between the other two variables. The statistical significance of the correlation coefficients among temperature, precipitation, and streamflow was computed using the bootstrap method (Efron, 1979) in the same way as for the Pearson correlation coefficient.

2.4. Wavelet analysis

Local and global wavelet power spectra were computed for streamflow, precipitation, and temperature. In this study we adopt the Morlet wavelet, which is given by

$$\psi_0(\eta) = \pi^{-1/4} e^{i\omega_0 \eta} e^{-\frac{1}{2}\eta^2}, \tag{2}$$

where ω_0 is the dimensionless frequency and η is the dimensionless time. Providing a balance between time and frequency localization, the Morlet wavelet with $\omega_0 = 6$ is recommended for identifying features of geophysical time series (Grinsted et al., 2004). To find the local wavelet power spectrum of a time series (x_n; $n = 1,\ldots, N$), such as streamflow or precipitation, one must take the wavelet transform of the time series, which is defined as

$$W_n^X(s) = \sqrt{\frac{\delta t}{s}} \sum_{n'=1}^{N} x_{n'} \psi_0 \left[\left(n' - n\right)\right] \frac{\delta t}{s}], \tag{3}$$

where δt is a uniform timestep (one month in this case), s is the scale of the Morlet wavelet, and $\eta = s \times t$. The more traditional Fourier period λ is approximately related to the wavelet scale by $\lambda = 1.03s$. The wavelet power at a given scale and time is then given by $\left|W_n^X(s)\right|^2$. Averaging $\left|W_n^X(s)\right|^2$ over the time index results in the global wavelet power spectrum. The significance of both global and local wavelet power at a given frequency and time can be tested against a red-noise background. The original time series can be reconstructed by taking the inverse wavelet transform of the wavelet coefficients (Torrence and Compo, 1998). In particular, to reconstruct the signal at a particular frequency, all wavelet coefficients are set to zero except for those corresponding to the frequency components of interest. Taking the inverse wavelet transform of the modified wavelet coefficients will produce the signal at the desired frequency or period with all other frequency components removed. The reader is referred to Torrence and Compo (1998) and Grinsted et al. (2004) for a more detailed discussion of the theory of wavelet analysis and significance testing used in this paper.

To quantify the relationships between climate modes and Mid-Atlantic streamflow, precipitation, and temperature as a function of frequency and time, a wavelet coherence analysis was conducted. Following Grinsted et al. (2004), the wavelet coherence between two time series X and Y is given by

$$R_n^2(s) = \frac{\left|S(s^{-1} W_n^{XY}(s)\right|^2}{S\left(s^{-1}\left|W_n^X(s)\right|^2\right) \times S\left(s^{-1}\left|W_n^Y(s)\right|^2\right)} \tag{4}$$

where $W_n^{XY}(s)$ is the cross-wavelet transform, defined as the product of the wavelet transform of X and the complex conjugate of the wavelet transform of Y, and S is a smoothing operator defined by $S(W_n(s)) = S_{\text{scale}}(S_{\text{time}}(W_n(s)))$. S_{time} represents smoothing in time and S_{scale} is smoothing along the wavelet scale axis. Eq. (4) resembles the definition of the correlation coefficient and, in fact, can be regarded as such. That is, a coherence value of 0 signifies that the two time series are unrelated, whereas a coherence value of 1 indicates the two time series are linearly related at the given frequency and time. For a phase θ and period λ, the phase lag is given by $\lambda\theta/\pi$.

Using Monte Carlo methods, the statistical significance of wavelet coherence was found by generating a large number of synthetic data pairs with the same lag-1 autocorrelation coefficients as the input time series, calculating the wavelet coherence for each pair, and then estimating the significance level at each scale using values outside the cone of influence (Grinsted et al., 2004). A more detailed discussion of wavelet coherence can be found in Grinsted et al. (2004).

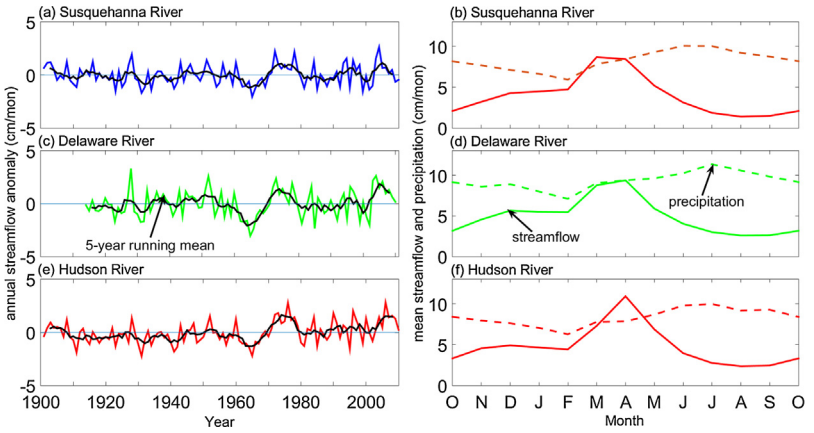

Fig. 2. Observed annually averaged (a) Susquehanna, (c) Delaware, (e) Hudson River streamflow anomalies and 5-year running mean of the observed time series for 1900–2010. Mean annual cycles of (b) Susquehanna River streamflow and SRB precipitation, (d) Delaware River streamflow and DRB precipitation, and (f) Hudson River streamflow and HRB precipitation for 1900–2010.

Characteristic timescales reported in this study were identified using global wavelet power spectra, the time-averaged representations of the sample wavelet power spectra. Periods of maximum time-averaged power were considered the dominant timescale of variability. For time-averaged wavelet coherence, however, an alternative definition was used, which is given by

$$G_C(s) = \frac{|W^{XY}(s)|^2}{\left(\sum_{n=1}^{N}|W_n^X|^2\right)\left(\sum_{n=1}^{N}|W_n^Y|^2\right)}, \tag{5}$$

where

$$W^{XY}(s) = \sum_{n=1}^{N} W_n^X(s)\, W_n^{Y*}(s), \tag{6}$$

with the asterisk denoting the complex conjugate (Elsayed, 2006). Eq. (5) measures the coherence between two time series in the entire study period at a scale s. Statistical significance of $G_C(s)$ was computed using Monte Carlo methods as follows: red-noise time series with the same lengths and lag-1 autocorrelation coefficients as the two input data series were generated and $G_C(s)$ was computed for each pair of red-noise time series. The resulting distribution of $G_C(s)$ at each scale was then used to estimate the significance of the global coherence estimates.

To quantify the impacts of climate modes on streamflow and precipitation variability, the quantity

$$F_n^X(s) = R_n^2(s)\, W_n^X(s), \tag{7}$$

representing the fraction of the power of X at n and s related to Y, was computed. In the present case, Y is a climate mode, the input into the system, and X is streamflow or precipitation, the linear response to Y. Before the above quantity was calculated, wavelet coherence values that were not statistically significant at the 5% level were set to zero, the idea being that insignificant wavelet coherence means that the null hypothesis cannot be rejected and the two time series at a given time and scale are considered independent (i.e., $R_n^2(s) = 0$). To obtain physical estimates of climate-mode impacts on streamflow and precipitation, the inverse transform of $F_n^X(s)$ was computed. If X^{mode} denotes the inverse transform of $F_n^X(s)$ for all time indices and scales, then X can be decomposed as

$$X = X^{\text{mode}} + X^{\text{residual}}, \tag{8}$$

where X^{residual} is the component of X unrelated to the climate mode. If $X = X^{\text{mode}}$, for example, then all of the time-series variability is due to forcing from the climate mode Y. It is noted that X^{residual} may not be purely noise, which would be the case if two independent climate modes were driving streamflow or precipitation.

3. Results

3.1. Observed variability of Mid-Atlantic streamflow, precipitation, and temperature

The observed annually averaged Susquehanna, Delaware, and Hudson River streamflow anomalies are shown in Fig. 2a, c and e, respectively. The variability in the time series from 1900 to 1940 was characterized by high-frequency oscillations,

Table 2
Linear Pearson correlation coefficients between climate indices and (a) Susquehanna River streamflow, (b) SRB precipitation, and (c) SRB temperature for 1950–2010. Only correlation coefficients significant at the 5% level are displayed, with correlation coefficients significant at the 1% level shaded in gray.

(a) Streamflow

	J	F	M	A	M	J	J	A	S	O	N	D		DJF	MAM	JJA	SON	Annual
NAO													NAO					
AO									0.34				AO					
AMO						−0.26				0.26			AMO			−0.26		
Nino 3.4		−0.30											Nino 3.4					
SO		0.27									−0.30		SO					
NPO						0.26			0.26		0.41		NPO				0.35	
PNA											−0.34		PNA				−0.30	−0.26
PDO													PDO					

(b) Precipitation

	J	F	M	A	M	J	J	A	S	O	N	D		DJF	MAM	JJA	SON	Annual
NAO													NAO					
AO													AO					
AMO						−0.26				0.49	−0.30		AMO					
Nino 3.4				0.38									Nino 3.4					
SO				−0.30							−0.30		SO					
NPO													NPO					
PNA				0.27									PNA					
PDO				0.33									PDO					

(c) Temperature

	J	F	M	A	M	J	J	A	S	O	N	D		DJF	MAM	JJA	SON	Annual
NAO	0.38	0.43	0.34	0.33						0.31		0.50	NAO	0.49				
AO	0.42	0.37	0.32	0.28						0.35	0.36	0.58	AO	0.53				
AMO													AMO				0.28	
Nino 3.4										−0.28			Nino 3.4				−0.25	
SO													SO					
NPO	0.29										0.32	0.33	NPO					
PNA	−0.30					−0.26			0.34		−0.29		PNA					
PDO	−0.30									−0.38	−0.39		PDO				−0.43	

whereas pronounced low-frequency variability as well as high-frequency variability occurred during 1960–1980. The low-frequency variability is evident by examining the five-year running mean of the time series (shown in black), which highlights the decadal variability of streamflow during the period 1950–1980. The 1960s drought and the pluvials (very wet periods) of the 1970s and 2000s are evident in all three basins. The 1960s drought was deepest in the DRB whereas the pluvials appear to have been greatest in the HRB. The mean annual cycles of streamflow and precipitation in the three basins are shown in Fig. 2b, d and f. The streamflow annual cycles are characterized by large maxima in spring, minima in summer, and a secondary maximum in late fall, extrema that are caused by the annual cycle in evapotranspiration and snowmelt—not precipitation, which has a weak annual cycle (e.g., Najjar, 1999). Unlike Susquehanna and Delaware River streamflow, Hudson River streamflow exceeded precipitation during April, possibly due to snowmelt during that month.

3.2. *Streamflow/precipitation-climate mode correlation analysis*

Panels a and b of Tables 2, 3, and 4 show the linear correlation analysis of streamflow-climate index and precipitation-climate index for the Susquehanna, Delaware, and Hudson Rivers, respectively. The Niño 3.4 index was found to be weakly correlated with Delaware River streamflow and DRB precipitation in April, accounting for approximately 16% of the variance of precipitation. A similar relationship was found for SRB precipitation and no relationships were identified for the HRB. A possible explanation for the increased April streamflow during positive Niño 3.4 phases is the increased January–March US East Coast storm frequency and subsequent increase in precipitation (Eichler and Higgins, 2006). The significant correlation coefficients with the SO and Niño 3.4 indices were generally similar and of opposite sign. There are a few notable exceptions: for example, November Susquehanna streamflow and HRB precipitation were not correlated with the Niño 3.4 index but were correlated with the SO index. Differences may be the result of how SSTs lag changes in the atmosphere.

Numerous statistically significant PNA-precipitation and PNA-streamflow relationships were found, consistent with the fact that the PNA tends to be in a positive phase during positive Niño 3.4 events (Feldstein, 2000). The April PNA index was found to be significantly and positively correlated with April precipitation for the DRB and SRB, though the PNA index was only significantly correlated with Delaware River streamflow. The streamflow-PNA and precipitation-PNA relationships may be the result of a southeastward-shifted trough that provides more favorable conditions for coastal storm development (Leathers et al., 1991). The PNA and the related NPO also had seasonal influences: the PNA and NPO indices were significantly

Table 3
Same as Table 2 but for the DRB.

(a) Streamflow

	J	F	M	A	M	J	J	A	S	O	N	D		DJF	MAM	JJA	SON	Annual
NAO										−0.32			NAO					
AO									0.34				AO					
AMO						−0.30				0.44			AMO				0.31	
Nino 3.4		−0.28		0.27									Nino 3.4					
SO					0.30								SO					
NPO				−0.34					0.25		0.28		NPO		−0.37		0.36	
PNA				0.39									PNA		0.36			
PDO				0.27				−0.25					PDO					

(b) Precipitation

	J	F	M	A	M	J	J	A	S	O	N	D		DJF	MAM	JJA	SON	Annual
NAO								0.25					NAO					
AO													AO					
AMO						−0.31				0.45			AMO				0.26	
Nino 3.4				0.37									Nino 3.4					
SO				−0.26	0.33								SO					
NPO				−0.29									NPO		−0.31		0.30	
PNA				0.38									PNA		0.34			
PDO				0.29									PDO					

(c) Temperature

	J	F	M	A	M	J	J	A	S	O	N	D		DJF	MAM	JJA	SON	Annual
NAO	0.37	0.41	0.32	0.30						0.28		0.53	NAO	0.50				
AO	0.41	0.36	0.31							0.39	0.36	0.56	AO	0.53		0.28		
AMO									0.30				AMO				0.30	
Nino 3.4										−0.26			Nino 3.4					
SO													SO					
NPO	0.25										0.33	0.27	NPO					
PNA	−0.25								0.30		−0.31		PNA					
PDO	−0.24									−0.39	−0.36		PDO				−0.42	

correlated with Delaware River streamflow and precipitation at the 1% level in spring and were also found to be significantly correlated with Susquehanna and Hudson River streamflow in fall.

It is noted that the NPO, PDO, and PNA indices were not found to be correlated with summer streamflow for all three rivers, though Barlow et al. (2001) found North Pacific SSTs, the so-called North Pacific mode (NPM), to be related to summer streamflow and drought conditions across the Northeast US. On the other hand, the modes were generally related to spring and fall streamflow, which were correlated with the SO and Niño 3.4. Differences between the results from Barlow et al. (2001) may be due to how the NPM, using EOF analysis, was statistically constrained to be independent from the PDO that was simultaneously derived from the same data set. In the present case, the NPO and PDO indices are not orthogonal but strongly correlated so that no independent information was gained.

In agreement with Xu et al. (2012), some PDO-streamflow associations were identified, particularly in April. The lagged relationship between Susquehanna streamflow and the PDO index found by Xu et al. (2012) may be an artifact of the autocorrelation inherent in the PDO time series and the PDO's relationship with the PNA and NPO. For example, the winter PDO index may be correlated with the subsequent fall PNA index, which was related to fall streamflow, resulting in the PDO index being correlated with future streamflow.

Linear correlation coefficients between streamflow and precipitation are shown in Fig. 3, where all the correlation coefficients are significant at the 5% level. For all three river basins, the streamflow-precipitation correlation coefficients reached local minima in February–April, July, and November; local maxima were found in May–June, August–October, and December. As shown in Fig. 2, precipitation equals streamflow in February and March for the DRB and SRB and yet the correlation coefficients reach local minima in those months, suggesting that some of the precipitation is falling as snow. The same arguments for the HRB hold in January and February but streamflow exceeds precipitation in March so that snowmelt may contribute to the low correlation coefficients in March and April. The minima in July for all three river basins may be due to large base-flow contributions and large evapotranspiration rates. Base-flow has a longer time-scale so that streamflow from prior months may be contributing to streamflow variability in subsequent months.

Perhaps the most interesting minima occurred in November, when there also may be a base-flow contribution in this month given the relatively low mean streamflow. However, the partial correlation coefficients between November precipitation and November streamflow with the effect of October streamflow removed showed that October streamflow contributed substantially to the observed November streamflow variability for all three basins. The effect was to reduce the simultaneous correlation between streamflow and precipitation. In fact, the difference between the linear correlation and partial correla-

Table 4
Same as Table 3 but for the HRB.

(a) Streamflow

	J	F	M	A	M	J	J	A	S	O	N	D		DJF	MAM	JJA	SON	Annual
NAO	0.26												NAO					
AO			0.30						0.32				AO					
AMO										0.31			AMO					
Nino 3.4													Nino 3.4					
SO													SO					
NPO									0.29				NPO				0.29	
PNA									−0.27				PNA					
PDO													PDO					

(b) Precipitation

	J	F	M	A	M	J	J	A	S	O	N	D		DJF	MAM	JJA	SON	Annual
NAO		0.26											NAO					
AO					0.32								AO					
AMO					−0.31					0.48	−0.39		AMO					
Nino 3.4		−0.32											Nino 3.4					
SO		0.27									−0.30		SO					
NPO													NPO					
PNA													PNA					
PDO		−0.28											PDO					

(c)Temperature

	J	F	M	A	M	J	J	A	S	O	N	D		DJF	MAM	JJA	SON	Annual
NAO	0.38	0.40					0.32			0.30		0.49	NAO	0.51				
AO	0.41	0.27					0.37			0.42	0.40	0.53	AO	0.52		0.37	0.31	
AMO									0.28				AMO				0.28	
Nino 3.4			0.29					−0.27					Nino 3.4					
SO			−0.30										SO					
NPO										0.27	0.34	0.26	NPO					
PNA									0.37	−0.25	−0.30		PNA					
PDO										−0.40	−0.37		PDO				−0.47	

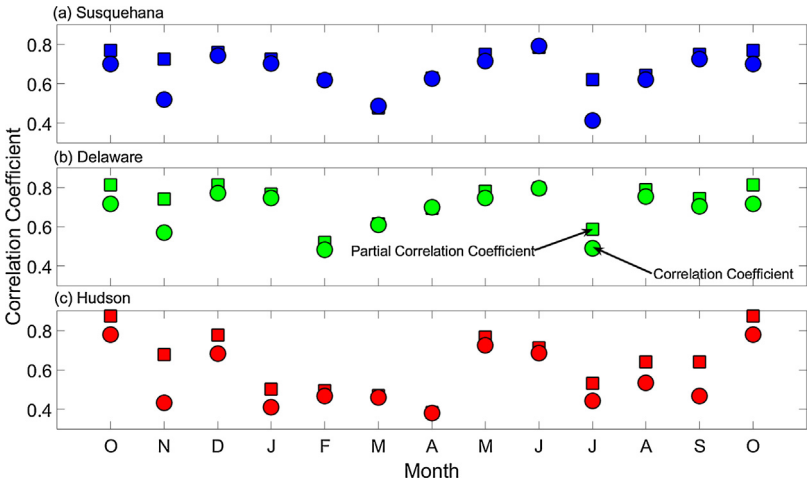

Fig. 3. Ordinary and partial correlation coefficients between mean monthly streamflow and precipitation for the Susquehanna, Delaware, and Hudson River basins for the period 1950–2010. The partial correlation coefficients account for the previous month's streamflow. All correlation coefficents are signifcant at the 5% level.

tion coefficients was generally greatest in the fall and summer for all three rivers basins, suggesting preceding streamflow is most important during the fall and summer. Physically, the stronger influence of preceding streamflow represents the larger groundwater component of streamflow.

In contrast to the seasonal time scale, streamflow and precipitation are highly correlated on the annual timescale, with the correlation coefficients between annual-mean streamflow and precipitation for 1950–2010 being 0.92, 0.95, and 0.85 for the SRB, DRB, and HRB, respectively, similar to previous analyses (Najjar, 1999; Najjar et al., 2009).

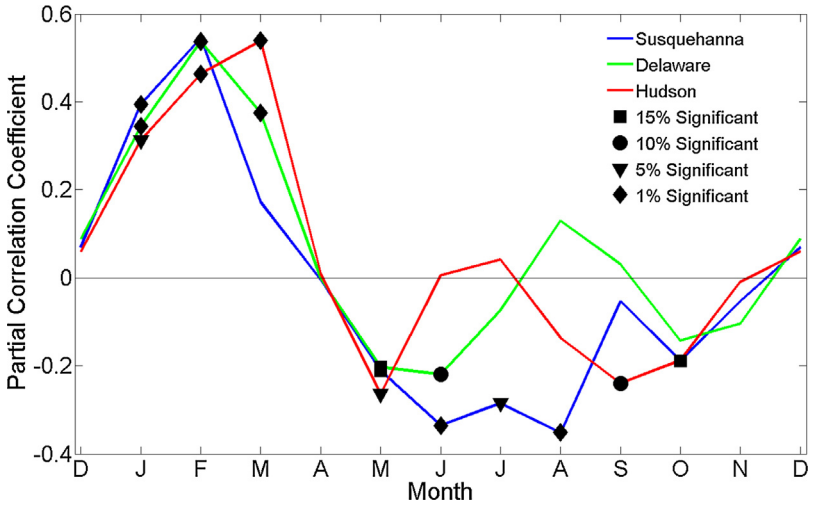

Fig. 4. Partial correlations coefficients between mean monthly maximum temperature and streamflow for the Susquehanna, Delaware, and Hudson Rivers for the period 1950–2010. Markers indicate the significance of the partial correlation coefficients.

3.3. Temperature-climate mode correlation analysis

Partial correlation coefficients (with the dependence of precipitation removed) between mean maximum temperature and streamflow are shown in Fig. 4. In general, temperature was positively and significantly partially correlated with streamflow during the cold season for all three river basins, consistent with the fact that winter precipitation type is strongly dependent on daily mean maximum temperature on precipitation days so that precipitation on cold days will fall as snow and contribute little to streamflow (Serreze et al., 1998). The negative relationships between temperature and streamflow during the summer are physically consistent with an increase in temperature leading to more evapotranspiration and less streamflow. Having been correlated with temperature, streamflow may also have been influenced by climate modes through temperature effects in addition to precipitation effects, motivating the temperature-climate mode analysis discussed next.

Tables 2–4c show the results of the temperature-climate index (simple) correlation analysis. The NAO index was found to be positively correlated with temperature, with the strongest influence occurring in the winter, when the atmosphere is most dynamically active and an enhanced jet and surface southerly flow associated with the positive NAO phase advects positive temperature anomalies across the Northeast US (Notaro et al., 2006). The positive correlation coefficients between the AO and temperature are a result of a positive AO phase being associated with fewer polar air outbreaks across North America (Thompson and Wallace, 2001), whereas the moderate temperature-PNA and temperature-NPO connections are the result of a deep Eastern-US trough during positive PNA and negative NPO phases (Leathers et al., 1991). A moderate correlation was identified between temperature and the PDO index in the fall, though no significant correlation coefficients were found with the PNA and NPO indices.

September Hudson River streamflow was negatively correlated to the PNA index but no precipitation-PNA association was identified. The PNA, however, was positively correlated with temperature during that month, and therefore the streamflow variability could possibly be related to PNA-related changes in temperature. The PNA-temperature relationships may also explain why, in November, the PNA index was significantly related to Susquehanna River streamflow and not to precipitation. A positive PNA index, being associated with lower-than-normal temperatures, may have resulted in more precipitation falling as snow, reducing November monthly streamflow. Note that the PNA index needs to only be related to precipitation type to affect streamflow. On the other hand, the precipitation-climate mode relationships could explain the April streamflow-climate mode associations found for the Delaware River because April streamflow was strongly correlated with April precipitation (Fig. 3) and was uncorrelated with April maximum temperature (Fig. 4). The ENSO-induced Delaware River streamflow variability is also associated with the concurrent changes in precipitation. Despite the moderate correlation between temperature and the indices for the AO and NAO, the NAO and AO were not found to be significantly correlated with winter streamflow.

3.4. Wavelet analysis

In order to detect the major frequencies of oscillation in the hydrometeorology of the Mid-Atlantic Region, we now present wavelet power spectra of SRB, DRB, and HRB streamflow and precipitation along with the corresponding global wavelet spectra (Figs. 5, 6, and 7).

The local power spectra revealed statistically significant streamflow variability at $\lambda = 26$ years in all three river basins from roughly 1940 to 2010 (Figs. 5a, 6a, and 7a). The global power spectra of streamflow also identified statistically significant

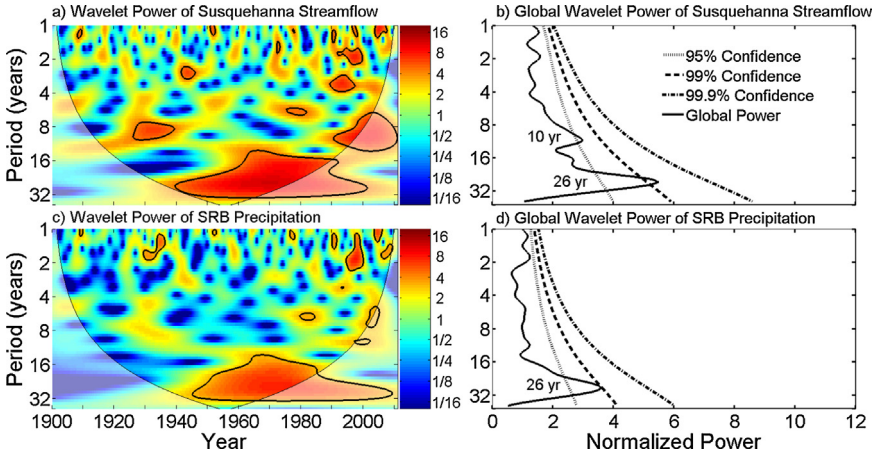

Fig. 5. (a) Normalized wavelet power spectrum of Susquehanna River streamflow from 1900 to 2010 together with the global wavelet power spectrum (b). (c) The normalized wavelet power spectrum of SRB precipitation together with the global wavelet power spectrum (d). Thick black contours in wavelet power spectra enclose areas of 5% significance against a red-noise background. Light shading represents the cone of influence. In the global power spectra, thick black lines represents the global wavelet power estimates and thin dashed black lines are the 95%, 99%, 99.9% confidence bounds against red-noise background spectra. Periods of peaks in the global power spectra exceeding 95% confidence are indicated.

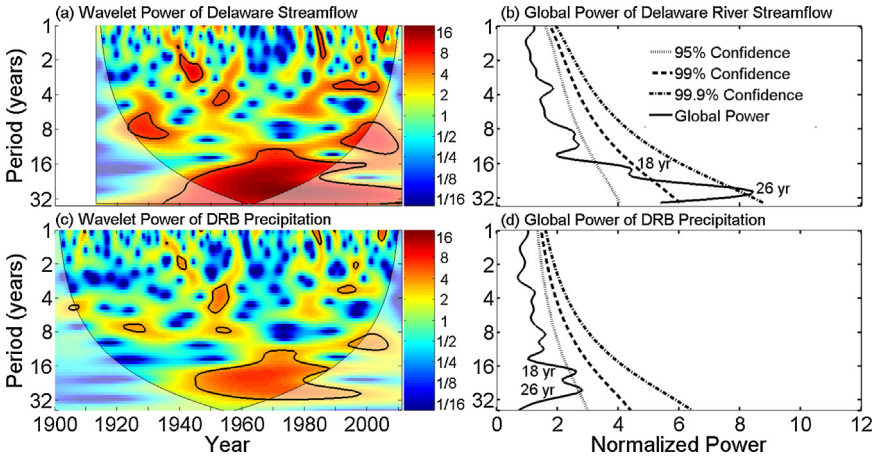

Fig. 6. Same as Fig. 4 but for the Delaware River Basin. Note that the streamflow record is shorter (1913–2010).

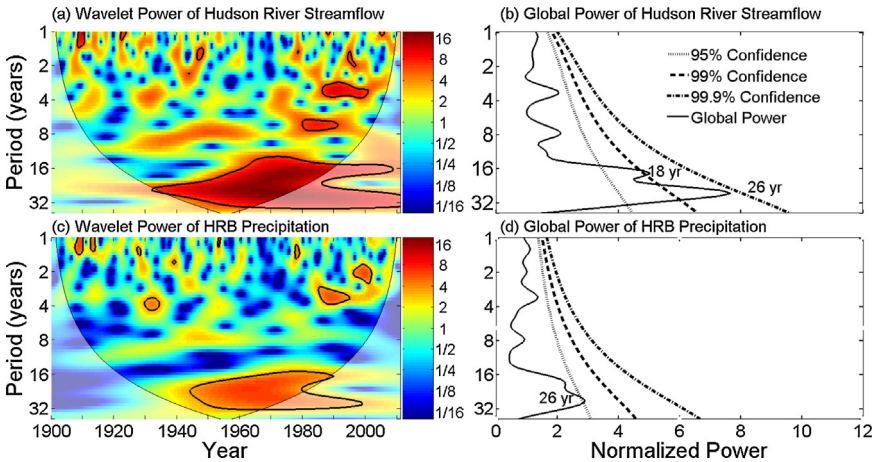

Fig. 7. Same as Fig. 4 but for the Hudson River Basin.

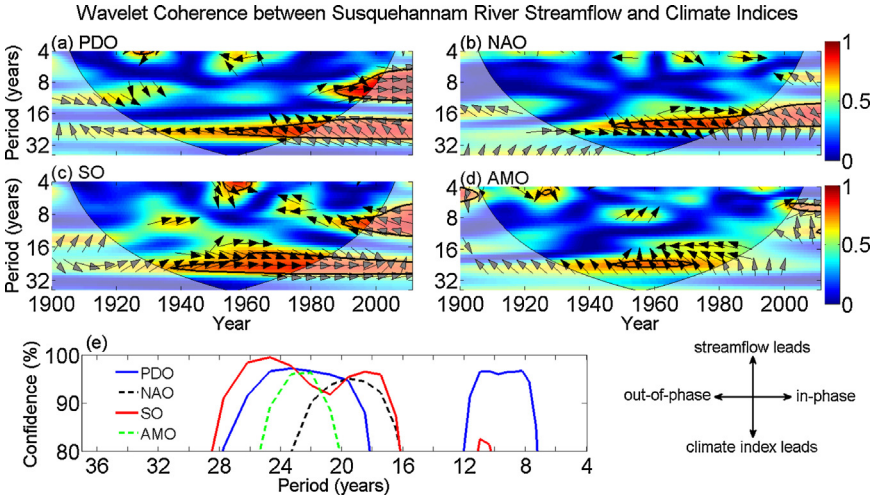

Fig. 8. (a) Wavelet coherence of monthly Susquehanna River streamflow and the (a) PDO, (b) NAO, (c) SO, and (d) AMO indices during 1900–2010. Thick black contours indicate significance at the 5% level and arrows indicate relative phase relationships (see legend in the lower right). Light shading represents the cone of influence. The wavelet coherence spectra were truncated to four years for clarity. Arrows are only plotted for those wavelet coherence values exceeding 0.55. (e) Significance of the 1900–2010 time-averaged wavelet coherence between streamflow and the climate indices.

wavelet power (Figs. 5b, 6b, and 7b). For the Hudson and Susquehanna Rivers, 1% significant peaks at $\lambda = 26$ years were identified, while a 0.1% significant peak at $\lambda = 26$ years was identified for the Delaware River (Figs. 5b, 6b, and 7b). Secondary peaks at $\lambda = 18$ years were also identified in the global wavelet spectrum of Hudson (1% significance) and Susquehanna (5% significance) River streamflow. The wavelet spectrum for Susquehanna River streamflow also contains a 5% significant peak at ~10 years, which was not found for the other two rivers. The wavelet power spectra suggest that the low-frequency fluctuations in streamflow were unlikely the result of a stochastic fluctuation and may be predictable. In other words, streamflow for the investigated rivers shifted between regimes of negative and positive anomalies every 13 years and such shifts were not random, occurring at regular intervals.

The wavelet power spectra of precipitation (panels c and d of Figs. 5, 6, and 7) are similar to the wavelet power of streamflow, suggesting that the streamflow variability was primarily driven by regional precipitation changes. This is not surprising given the strong correlation between annual-mean streamflow and annual-mean precipitation noted earlier (Section 3.2). The statistical significance of the peaks, however, are lower, especially for HRB and DRB precipitation, where the peaks at $\lambda = 26$ years only exceed the 5% significance level (Figs. 5d, 6d, and 7d). The peak at $\lambda = 26$ years for Susquehanna River streamflow is nearly significant at the 1% level. There is also a secondary peak at ~18 years for the DRB not found for the SRB or HRB, though a similar peak was found in the global spectra for Hudson River streamflow.

The results from the wavelet analysis of temperature (not shown) identified no significant decadal variability for all three river basins and support the idea that streamflow variability at the decadal timescale was mainly driven by precipitation changes.

3.5. *Wavelet coherence analysis*

Local and global wavelet coherence spectra show that the PDO, AMO, NAO, and SO are coherent with Susquehanna River streamflow at a variety of timescales (Fig. 8). Wavelet coherence spectra for the Niño 3.4 index and NPO index are not shown for any of the basins because the Niño 3.4 results are nearly identical to those for the SO and the NPO results reveal no significant coherence. The PDO, NAO, and SO were found to be coherent with Susquehanna River streamflow at multi-decadal timescales, mainly in the latter half of the record. The wavelet coherence analysis detected a 7-year lagged (i.e., streamflow leads) relationship with the PDO at $\lambda = 23$ years from 1950 to 2010, an in-phase relationship between streamflow and the SO at $\lambda = 25$ years extending from 1940 to 2010, and a 2-year lagged relationship with the NAO at 20 years extending from 1950 to 2010. The peaks were inferred from the significance of global coherence as shown in Fig. 8e The AMO has a multidecadal peak ($\lambda = 23$ years in the global spectra), which reflects local coherence in the 1950s and 1960s. The secondary peak in SO global coherence significance at $\lambda = 18$ years suggests that the region of local coherence in Fig. 8c at $\lambda = 25$ years is actually the merger of two separate peaks. The SO and the PDO also show peaks in the global spectra at around 10 years, which are presumably related to local spectra significance since approximately 1990. The phases are roughly opposite to those corresponding to the ~20-year periods, the implications of which will be discussed in Section 4.

Wavelet coherence between SRB precipitation and climate modes (Fig. 9) are broadly similar to spectra between Susquehanna River streamflow and climate modes, with both coherence spectra having significant (95% confidence) peaks for the SO at approximately 18 and 26 years and for the PDO at about 10 and 20 years. However, the AMO and NAO peaks, significant in the streamflow global coherence spectra, have less than 85% confidence in the corresponding precipitation spectra.

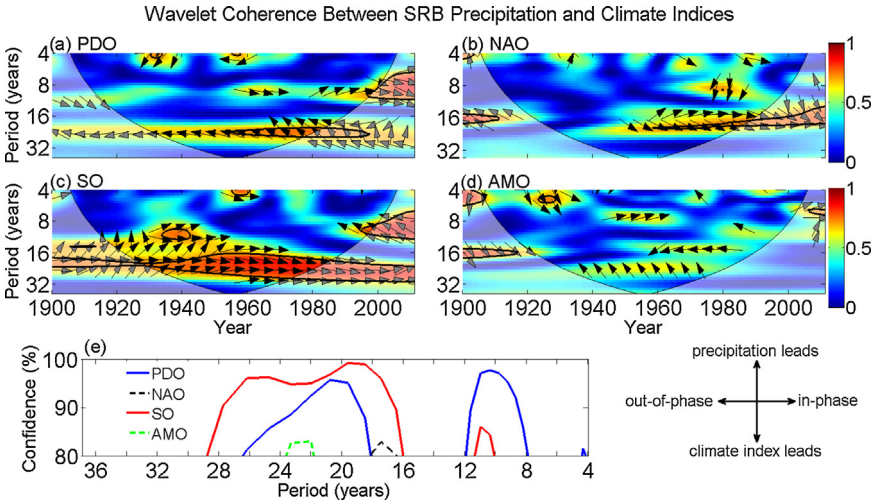

Fig. 9. Same as Fig. 8 but for Susquehanna River Basin precipitation.

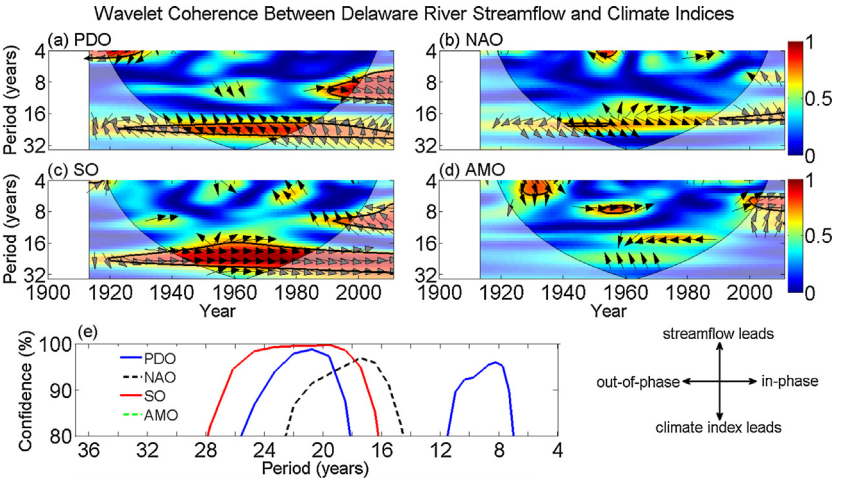

Fig. 10. Same as Fig. 8 but for Delaware River streamflow for 1913–2010.

Wavelet coherence results for the DRB (Figs. 10 and 11) were broadly similar to those for the SRB in terms of dominant periods, phase relationships, and temporal variability, except that the significance in the local spectra for the PDO and SO at ~20 years extended from 1920 to 2010. As with the SRB, the coherence between streamflow and climate modes was similar to that between precipitation and climate modes, except that precipitation generally had a greater response to the PDO and SO at ~20 years, suggesting that another mechanism may be weakening the response of streamflow to the climate modes. The local coherence significance region extending from 1980 to 2010 corresponding to local coherence between the SO and streamflow at ~10 years for the SRB is also present for the DRB, with the same out-of-phase relationship as the SRB. The PDO streamflow relationships at ~10 years were found to be identical. In particular, the local coherence spectra for SRB and DRB precipitation contain significance regions at ~10 years (extending from 1980 to 2010), which are similar and smaller than those for streamflow. The differences indicate that another mechanism enhanced the streamflow response to the PDO, unlike the responses at ~20 years. The difference between the streamflow and precipitation response to the PDO is not, however, evident in global coherence spectra for the SRB, unlike for the DRB, where the confidence of peak for precipitation is approximately 5% less. Statistically significant global coherence between Delaware River streamflow and the NAO index at $\lambda = 17$ years was also identified, though locally little statistical significance was found. No global or local statistically significant NAO-precipitation relationships were detected. At both 10 years and 20 years the precipitation-PDO and precipitation-SO relationships were similar to the streamflow-climate mode relationships, suggesting that precipitation was the primary driver of the multi-decadal streamflow variability, which is influenced by the PDO and SO.

The wavelet coherence between the four climate modes and Hudson River streamflow is shown in Fig. 12. The wavelet coherence analysis detected a statistically significant coherent and in-phase SO-streamflow relationship at $\lambda = 25$ years extending from 1930 to 2010, as indicated by the peak in local and global coherence (Fig. 12e). A period of significant

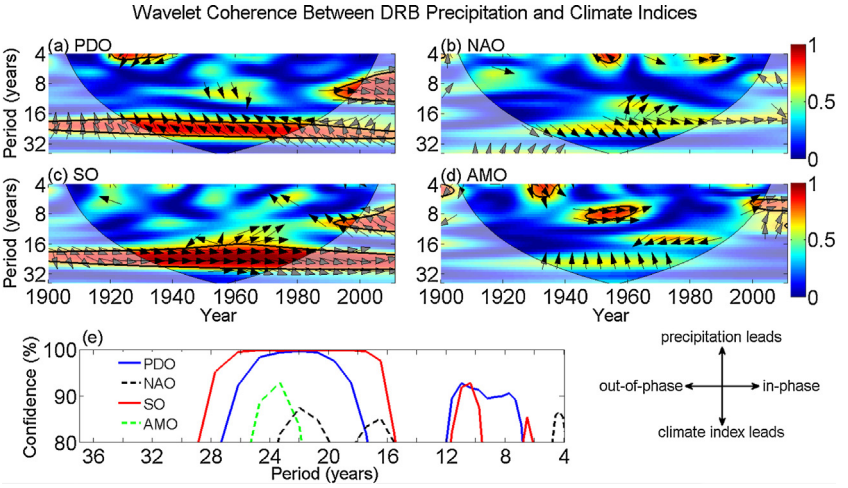

Fig. 11. Same as Fig. 8 but for Delaware River Basin precipitation.

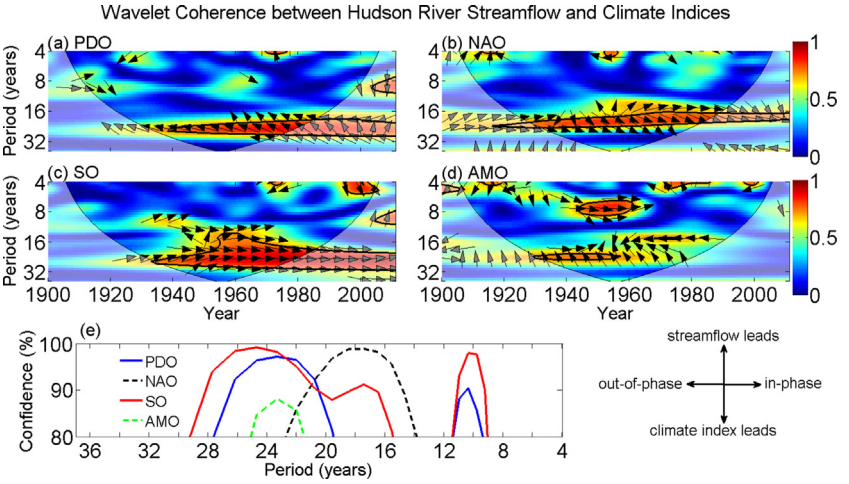

Fig. 12. Same as Fig. 8 but for Hudson River streamflow.

coherence between the PDO and streamflow extending from 1940 to 2010 was also identified at $\lambda = 23$ years, with streamflow lagging by 7 years. The results were similar to those for the other rivers except that the Hudson River streamflow relationship with the SO was stronger than the Susquehanna-SO relationship. The global coherence spectra indicate that the SO was more coherent with Hudson River streamflow than with streamflow of the other rivers at $\lambda = 10$ years. It is also noted that the HRB precipitation response to the PDO and SO is stronger than the streamflow response, implying that another mechanism is operating to weaken the streamflow response.

One commonality between the HRB and SRB is the NAO-streamflow relationships; little statistically significant local coherence was found for the DRB, whereas both Hudson and Susquehanna River streamflow were both significantly coherent with the NAO at ~18 years. The commonality also exists in the local coherence spectra for precipitation but is less evident. A transient relationship between precipitation and the AMO in the HRB—not existing in the local coherence spectra for the DRB and SRB—was also found in the period band of 6–8 years from 1900 to 1960. A corresponding peak in the global coherence was also identified, which was also not found for the DRB and SRB.

It is possible that the observed streamflow variability at a period of 20 years was partially due to temperature variability. The wavelet coherence between climate indices and temperature for each river basin was therefore computed (not shown). For the SRB no significant wavelet coherence with temperature and the SO and AMO indices at a period of 20 years was found. On the other hand, significant out-of-phase coherence was found with the PDO index at a period of 20 years, suggesting that the positive phase of the PDO contributes to drier and cooler conditions across the Northeast US at that timescale. Namias (1966) also found the 1960s drought to be accompanied by below-normal temperatures associated with a prevailing northerly wind component. Identical relationships with the PDO index were found for the DRB and HRB and little to no significant coherence was found with the other climate indices. The out-of-phase relationship between the PDO

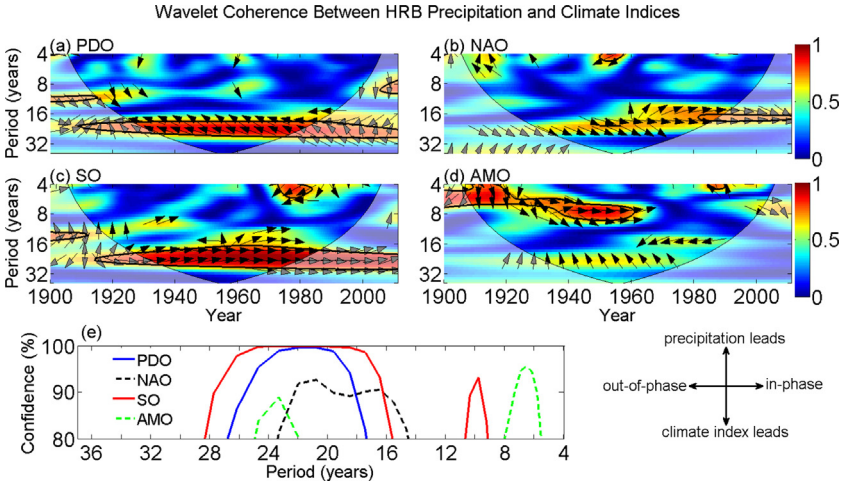

Fig. 13. Same as Fig. 8 but for Hudson River Basin precipitation.

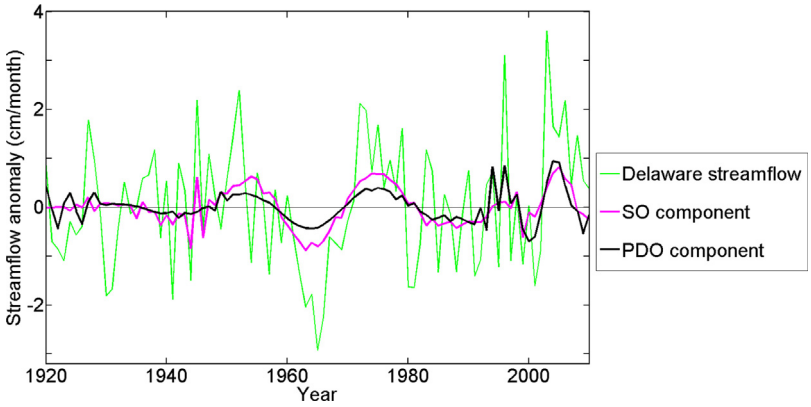

Fig. 14. The observed annually averaged Delaware River streamflow anomalies and the PDO and SO components of the observed time series for 1920–2010.

Table 5
Contribution of the Southern Oscillation and the Pacific Decadal Oscillation to streamflow anomalies during the 1960s drought and the pluvials of the 1970s and 2000s.

Time period	Basin	Streamflow anomaly (cm mon^{-1})	SO contribution (%)	PDO contribution (%)
1963–1968	SRB	−1.0	37	13
	DRB	−1.8	40	21
	HRB	−1.2	54	27
1971–1979	SRB	1.0	33	25
	DRB	1.1	49	27
	HRB	1.4	35	23
2002–2007	SRB	0.9	50	57
	DRB	1.4	36	32
	HRB	1.0	19	14

and temperature could explain the weaker response of streamflow to the PDO for the DRB and HRB; cooler conditions would favor more streamflow on longer-scales, opposing the drying effects caused by the lack of rainfall Fig. 13.

3.6. *Impact of climate modes on low-frequency variability of streamflow*

The PDO and SO components of mean annual anomalies of Delaware streamflow, estimated using Eq. (7), are shown in Fig. 14 from 1920 to 2010, when large, low-frequency fluctuations were present. These climate modes appear to have contributed substantially to the 1960s drought and the pluvials of the 1970s and 2000s. To quantify the contributions of these two climate modes to the three aforementioned hydrometeorological events, the mean streamflow anomaly for the periods 1963–1968, 1971–1979, and 2002–2007 was computed for the SO component, the PDO component, and the observed time series for the Susquehanna, Delaware, and Hudson Rivers (Table 5). For the 1960s drought, the SO and PDO

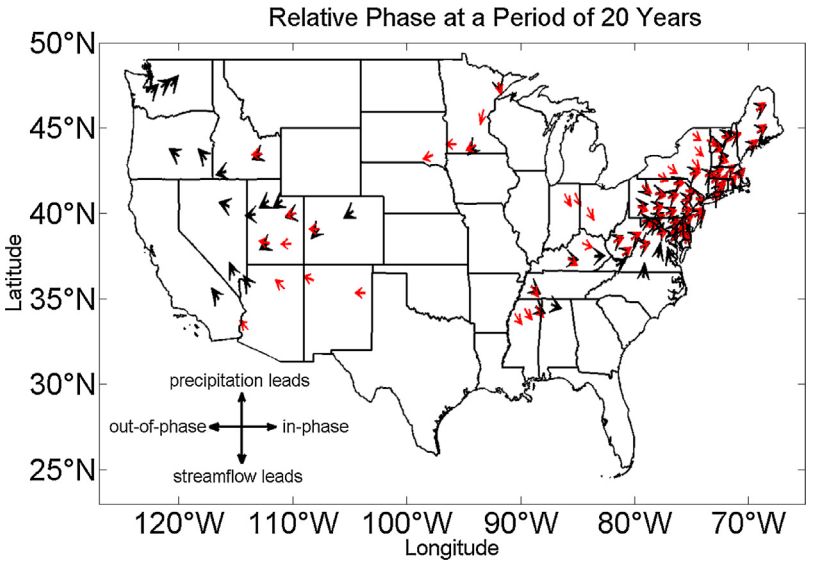

Fig. 15. The relative phase relationship between the SO index and Delaware River streamflow at a period of 20 years shown with black arrows and the relative phase relationship between the SO index and US climate divisional precipitation anomalies at a period of 20 years shown with red arrows. Calculations are for the 1913–2010 period and arrows are located at the centroids of the climate divisions for which the global coherence was significant at the 5% level. (For interpretation of the references to colour in this figure legend, the reader is referred to the web version of this article.)

contributions were greatest for the Hudson and lowest for the Susquehanna, being roughly a factor of two larger for the Hudson; the SO contributions were about twice those of the PDO. Note that the contributions of the SO and PDO may not be independent because of the close relationship between these two climate modes (Newman et al., 2003). The impact of the PDO and SO on the subsequent wet period 1971–1979 was similar for all three rivers but was greatest for Delaware River. The PDO's contribution was also smaller compared to the SO contributions for all three rivers. Similarly, the SO and PDO contributed approximately equally to the pluvial of the 2000s, with the Susquehanna being most influenced and the Hudson the least. In fact, the contributions differed by more than a factor of two, opposite to the climate-mode contributions to the 1960s drought. Results for precipitation (not shown) were similar to those for streamflow, indicating that the climate modes influenced streamflow during these hydrometeorological events mainly through precipitation. In addition to the SO and PDO, the analyses presented in Fig. 14 and Table 5 were conducted for the NAO, NPO, AMO, and Niño 3.4 indices. No substantial contributions to the 1960s drought and pluvials of the 1970s and 2000s were found for the NAO, NPO, and AMO; Niño 3.4 results were very similar to those for the SO.

3.7. Teleconnection analysis

Among all of the climate modes, the Southern Oscillation appears to have the greatest influence on Mid-Atlantic streamflow. Further, the SO influence is greatest at a period of approximately two decades. To investigate a possible teleconnection influence of the SO on Mid-Atlantic streamflow, a wavelet coherence analysis was conducted between the SO index and climate-division precipitation. The phase of the SO-precipitation relationship at a period of 20 years for each climate division is indicated by black arrows in Fig. 15 when the global coherence exceeds the 5% significant level. The SO-precipitation relationship was found to be in-phase across the eastern US, with statistically significant global coherence limited to the Northeast. A remote region of significant global coherence is also present in the Western and Southern US but the phase relationship is opposite to that of the Northeast. A similar analysis was conducted between Delaware River streamflow and climate-division precipitation (red arrows). Remarkably, it was found that the global coherence spatial pattern was nearly identical to the SO-precipitation associations. The remote region of significant global coherence in the West is suggestive of a teleconnection pattern, with wet conditions in the Western US being accompanied by drier conditions in the East. In fact, Namias (1966) noted that while the Northeast was dry during the period 1962–1966, the Southwest and Northern plains were wet, generally consistent with the results presented in Fig.15. Seager et al. (2005) found, using a general circulation model, that tropical SSTs can produce the Dust Bowl in the 1930s for the Southwestern US, but Seager et al. (2012) showed that the models cannot produce the 1960s drought in the Northeastern US. However, Fig. 15 implies that Delaware River streamflow is phase-locked to Southwestern US precipitation and so must also be phase-locked to tropical SSTs that forced precipitation variability in that region.

The relative phase relationship between DRB precipitation and 500-hPa geopotential height anomalies at a period of 20 years is shown in Fig. 16a. The figure shows regions of statistically significant global coherence as indicated by contours with corresponding opposite phase relationships. The alternating phase relationships suggest that DRB precipitation at a period

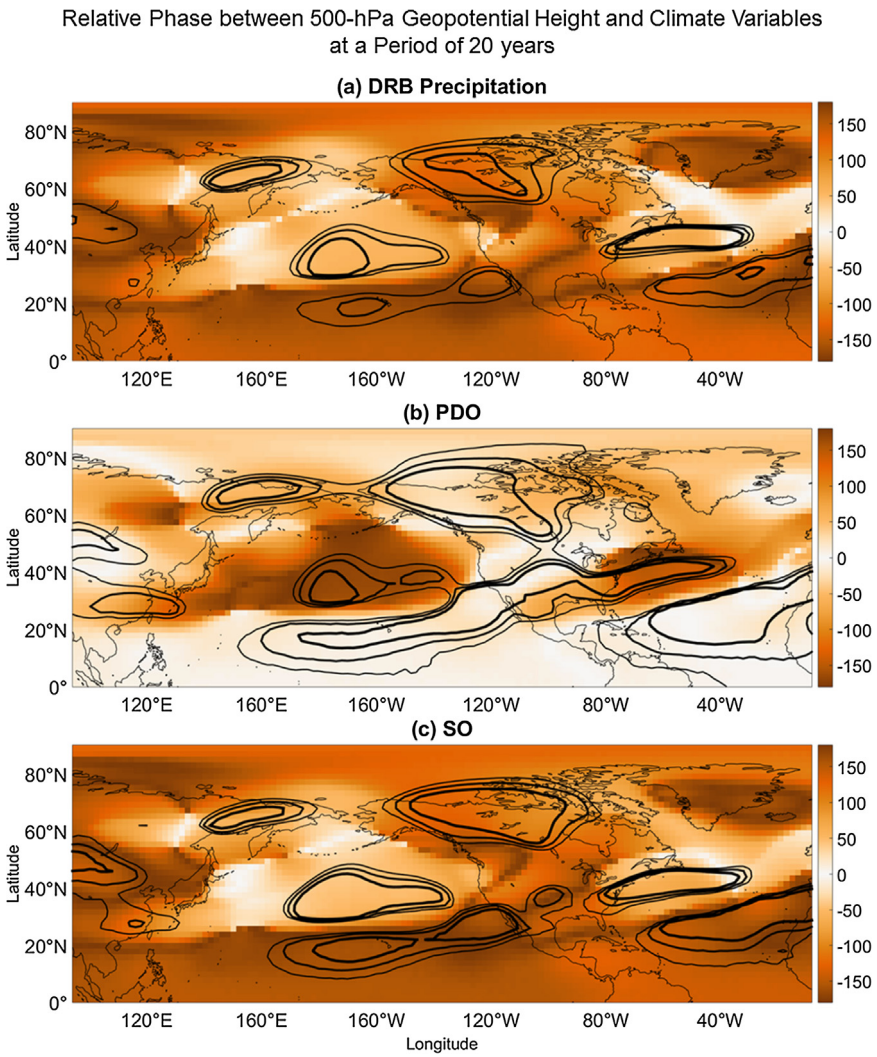

Fig. 16. (a) Relative phase difference between 500-hPa geopotential height and DRB precipitation, (b) between 500-hPa geopotential height and the PDO index, and (c) between 500-hPa geopotential height and the SO index at a period of 20 years. Thin contours enclose regions of 15% statistically significant global coherence, medium-weighted contours enclose regions of 10% statistical significance, and the thickest contours enclose regions of 5% statistical significance.

of 20 years was related to a Rossby wave train emanating from the tropical North Pacific Ocean, which arced over North America. Such a Rossby wave response is consistent with the mid-latitude response to tropical thermal forcing (Hoskins and Karoly, 1981). The Rossby wave train, moreover, explains why DRB precipitation fluctuated coherently with Southwest US precipitation at a period of 20 years. The SO and PDO indices were also found to have been synchronized with 500-hPa geopotential height anomalies in a similar manner to DRB precipitation, which suggests that the PDO and SO were related to the global circulation pattern that was linked to the 20-year variability of DRB precipitation.

4. Discussion

The AMO, NAO, PDO, and the SO were found to be contributors to decadal to multi-decadal variability of streamflow in the Mid-Atlantic region of the US. The wavelet coherence analysis identified the PDO and the SO as being the main regulators of the enhanced 26-year streamflow and precipitation variability identified in the wavelet power analysis. As noted by Mantua (2010), the PDO is most energetic at periods of 15–25 years and 50–70 years, which could explain why the PDO is most coherent with precipitation at a period of 22–24 years. Whitney (2010) speculated that the NAO could be responsible for the 26-year periodicity. However, our analysis clearly shows that the NAO plays a minor role while the PDO and the SO play a major role. Variability of Susquehanna River streamflow at low-frequencies was also noted by Labat (2008), who revealed statistically significant periodicities at periods of 3, 12, and 27 years using a global wavelet analysis. Though Labat (2008) and Whitney (2010) did not analyze precipitation, the findings from this study suggest that the 26–27 year streamflow

periodicities identified in these studies were driven by precipitation changes related to the SO and PDO, and to a lesser extent, the NAO.

Labat (2010), using a cross-wavelet analysis, determined that the PDO was driving North American continental freshwater discharge variability at a period of 22 years, a result similar to that found in this study (despite the very different study regions considered). However, this study added the phase relationship. Labat (2010) found the SO to have a weaker relationship at 21 years with North American continental freshwater discharge. It is important to note that, while the PDO and ENSO are regarded as distinct phenomena, the PDO is dependent on ENSO. According to Newman et al. (2003), the PDO may be regarded as the reddened response of atmospheric noise and ENSO, which could be problematic when separating pure ENSO and PDO signals in North American drought and climate proxies. Numerous studies have analyzed the connection between North Pacific SSTs and ENSO (Bjerknes, 1969; Luksch and von Storch, 1992; Trenberth and Hurrell, 1994; Nath and Lau, 1996), further supporting the similarity between the streamflow-PDO and streamflow-SO relationships as identified in our wavelet coherence analysis. According to Latif and Barnett (1996), SST anomalies in the North Pacific undergo a 20-year oscillation involving the interaction between the Aleutian Low and the subtropical gyre. This model suggests that a positive SST anomaly in the North Pacific resulting from an anomalously strong subtropical gyre weakens the Aleutian Low, which alters air-sea heat fluxes, reinforcing the initial SST anomaly set up by the subtropical gyre. Changes in the wind stress curl associated with the atmospheric response to the SST anomalies, however, act to spin down the subtropical gyre, reversing the initial temperature anomaly, with the oceanic response lagging the changes in wind stress curl. It is the interaction between the Aleutian Low and subtropical gyre that generates a 20-year oscillation, which coincides with the period at which the PDO is most coherent with Northeast US streamflow and precipitation, providing a possible physical mechanism for the PDO-streamflow teleconnection.

The similarity between the streamflow-SO and the streamflow-PDO relationships can be interpreted using the "atmospheric bridge" concept (Alexander, 2002). The essential component of the atmospheric bridge is the anomalously strong Aleutian Low during El Niño phases (Bjerknes, 1969), which alters heat fluxes, Ekman transport, and the ocean mixed layer depth, resulting in negative SST anomalies in the central North Pacific (Nath and Lau, 1996). Low SSTs in the central North Pacific contribute to a positive phase of the PDO and thus similarities between the streamflow-PDO and streamflow-SO relationships are expected.

A common theme from the wavelet analysis is the relationship between streamflow and four dominant modes on the ~20 year timescale. Even the less-coherent streamflow-NAO and streamflow-AMO relationships have a preferred timescale similar to the SO and PDO. Perhaps this is due to the link of the AMO and NAO with ENSO. For example, several studies have related NAO variability to SO variability and Atlantic Ocean SSTs to ENSO through Ekman pumping, ocean dynamics, and surface heat fluxes (e.g., Alexander et al., 2002). Furthermore, some studies suggest that the AMO may also influence the NAO and the PDO (Higuchi et al., 1999; Czaja and Frankignoul, 2002; Zhang and Delworth, 2007). Finally, solar activity may be responsible for the similarity in the wavelet coherence spectra. For example, Velasco and Mendoza (2008) found that solar activity influences the AMO, PDO, SO and the NAO at a 22-year timescale. Hence it is not surprising that a similar timescale was found for all climate indices in the wavelet coherence analysis. However, the SO and PDO have much stronger coherence with Mid-Atlantic streamflow than the NAO and AMO do.

Our finding on the connection between the SO and the 1960s drought contrasts with that of Seager et al. (2012), who attributed it to internal atmospheric variability. The contrasting results may be due to differences in statistical approaches; Seager et al. (2012) only considered the correlation between Northeast US seasonal precipitation and North American precipitation and concluded that Northeast precipitation was only locally correlated so that teleconnections were unlikely during any season. In contrast, in the present study, a correlation pattern suggestive of a teleconnection pattern was identified at a period of 20 years, where precipitation in the Southwestern US fluctuated coherently with Northeast precipitation. Another potential problem in Seager et al. (2012) is the exclusive use of standard correlation coefficients. A standard correlation coefficient quantifies the linear relationship between two time series on all timescales simultaneously, ignoring the fact that the phase relationships between two time series at one timescale can be opposite to a phase relationship at a another timescale. Fig. 11, as an example, shows that at a period of 20 years the SO is in-phase with DRB precipitation, whereas at period of 10 years it is out-of-phase with precipitation. Effects at the two timescales could cancel each other, resulting in a low overall correlation coefficient, even though the relationships are strong at particular timescales.

Seager et al. (2012) also base their conclusions on atmospheric global circulation model (GCM) simulations with prescribed SSTs, but uncertainties in the representation of convection in GCMs can manifest as false simulations of precipitation, particularly in terms of spatial patterns and variance (Peters et al., 2013). The uncertainties in convection and cloud feedback were also noted by Randall et al. (2007) and represent some of the largest problems in the latest GCMs. Given that the Northeast US given is relatively small, an accurate determination of the spatial pattern of precipitation is critical; small errors in the locations can produce large differences among GCM ensembles. The 1930s drought, for example, can be reproduced by forcing the GCM with SSTs during that period but the drought center is too far south (Cook et al., 2008). The statistical analysis of historical data in this study provides compelling evidence that the 1960s drought was externally forced, with precipitation anomalies fluctuating coherently with those across the Southwestern US, a region where tropical influences on drought have already been documented (Seager et al., 2005).

Climate models are in disagreement with how ENSO will respond to climate change. Some models suggest that more El Niños will occur and other models suggest more La Niñas will be preferred (Latif and Keenlyside, 2008). The uncertainties in the future behavior of ENSO may lead to uncertainties in Northeast US precipitation projections. If more La Niñas are favored

in the future, then, according to the results from the wavelet analysis, more frequent wet conditions will be preferred. On the other hand, if El Niños become more frequent so will drought conditions across the Northeast US. Thus, uncertainties in climate model projections of ENSO currently pose a great challenge in understanding future changes in regional precipitation variability.

5. Conclusions

Streamflow, precipitation, and temperature variability in the Mid-Atlantic region of the US was analyzed and linked to dominant modes of climate variability at annual to multi-decadal timescales. The influence of climate modes on precipitation, temperature, and streamflow were found to vary from month to month and from season to season. Moreover, correlation coefficients were generally similar for the three river basins considered here. The streamflow-climate mode relationships, precipitation-climate mode relationships, and temperature-climate mode relationships can be physically attributed to alterations in storm tracks, jet-stream positions, and prevailing winds, all of which affect the air mass characteristics across the Mid-Atlantic region. Both streamflow and precipitation showed significant variability at a period of 26 years as revealed by wavelet power spectra. Moreover, such periodicities could not be attributed to red-noise; rather, it was the result of ENSO and the PDO. The SO explains 37–54% of the streamflow decline across the Mid-Atlantic region during the 1960s drought, 33–49% of the 1970s pluvial, and 19–50% of the 2000s pluvial. It is therefore important for hydrological and climate studies to include such oscillations when assessing future impacts of climate change on the hydrology and ecology of the Hudson, Susquehanna, and Delaware watersheds and their receiving estuaries. It is hoped that the results from this study will aid hydrological and climate forecasts so that predictions about the future state of hydrological systems such as rivers and estuaries under a changing global climate system can be more accurately assessed.

Acknowledgements

Support for this research was provided by the National Science Foundation Physical Oceanography Program (award number 0961423) and the Hudson River Foundation (award number GF/02/14). The manuscript was improved by comments from two anonymous reviewers. We thank Sukyoung Lee for helpful discussions regarding tropically based teleconnections.

Appendix A. Supplementary data

Supplementary data associated with this article can be found, in the online version, at http://dx.doi.org/10.1016/j.ejrh.2015.11.003.

References

Alexander, M.A., Bladé, I., Newman, M., Lanzante, J.R., Lau, N., Scott, J.D., 2002. The atmospheric bridge: the influence of ENSO teleconnections on air–sea interaction over the global oceans. J. Clim. 15, 2205–2231.
Archambault, H.M., Bosart, L.F., Keyser, D., Aiyyer, A.R., 2008. Influence of large-scale flow regimes on cool-season precipitation in the northeastern United States. Mon. Weather Rev. 136, 2945–2963.
Barlow, M., Nigam, S., Berbery, E.H., 2001. ENSO, Pacific decadal variability, and US summertime precipitation, drought, and streamflow. J. Clim. 14, 2105–2128.
Barnston, A.G., Livezey, R.E., 1987. Classification, seasonality and persistence of low-frequency atmospheric circulation patterns. Mon. Weather Rev. 115, 1083–1126.
Bjerknes, J., 1969. Atmospheric teleconnections from the equatorial Pacific. Mon. Weather Rev. 97, 163–172.
Bradbury, J.A., Dingman, S.L., Keim, B.D., 2002. New England drought and relations with large scale atmospheric circulation patterns. J. Am. Water Resour. Assoc. 38, 1287–1299.
Cook, B., Miller, R.L., Seager, R., 2008. Amplification of the North American Dust Bowl drought through human-induced land degradation. Proc. Natl. Acad. Sci. U. S. A. 106, 4997–5001.
Compo, G.P., Whitaker, J.S., Sardeshmukh, P.D., Matsui, N., Allan, R.J., Yin, X., Gleason, B.E., Vose, R.S., Rutledge, G., Bessemoulin, P., Brönnimann, S., Brunet, M., Crouthamel, R.I., Grant, A.N., Groisman, P.Y., Jones, P.D., Kruk, M., Kruger, A.C., Marshall, G.J., Maugeri, M., Mok, H.Y., Nordli, Ø., Ross, T.F., Trigo, R.M., Wang, X.L., Woodruff, S.D., Worley, S.J., 2011. The twentieth century reanalysis project. Q. J. Roy. Meteorol. Soc. 137, 1–28.
Dettinger, M., Diaz, H., 2000. Global characteristics of streamflow and flow seasonality and variability. J. Hydrometeorol. 1, 289–310.
Efron, B., 1979. Bootstrap methods: another look at the jackknife. Ann. Statist. 7, 1–26.
Eichler, T., Higgins, W., 2006. Climatology and ENSO-related variability of North American extratropical cyclone activity. J. Clim. 19, 2076–2093.
Elsayed, M.A.K., 2006. A novel technique in analyzing non-linear wave–wave interaction. Ocean Eng. 33, 168–180.
Enfield, D.B., Mestas-Nuñez, A.M., Trimble, P.J., 2001. The Atlantic multidecadal oscillation and its relation to rainfall and river flows in the continental US. Geophys. Res. Lett. 28, 2077–2080.
Feldstein, S.B., 2000. The timescale, power spectra, and climate noise properties of teleconnection patterns. J. Clim. 13, 4430–4440.
Gershunov, A., Barnett, T.P., 1998. Interdecadal modulation of ENSO teleconnections. Bull. Am. Meteorol. Soc. 79, 2715–2725.
Grinsted, A., Moore, J.C., Jevrejeva, S., 2004. Application of the cross wavelet transform and wavelet coherence to geophysical time series. Nonlin. Processes Geophys. 11, 561–566.
Guttman, N.B., Quayle, R.G., 1996. A historical perspective of US climate divisions. Bull. Am. Meteorol. Soc. 77, 293–303.
Hoskins, B.J., Karoly, D.J., 1981. The steady linear response of a spherical atmosphere to thermal and orographic forcing. J. Atmos. Sci. 38, 1179–1196.
Hurrell, J.W., Kushnir, Y., Ottersen, G., Visbeck, M. (Eds.), 2003. The North Atlantic Oscillation: Climatic Significance and Environmental Impacts. Geophys. Monogr. Ser., vol. 134. American Geophysical Union, Washington, D.C.
Kerr, R.A., 2000. A North Atlantic climate pacemaker for the centuries. Science 288, 1984–1985.
Kreeger, D., Adkins, J., Cole, P., Najjar, R., Velinsky, D., Conolly, P., Kraeuter, J., 2010. Climate Change and the Delaware Estuary: Three Case Studies in Vulnerability Assessment and Adaptation Planning Tech. Rep. Partnership for the Delaware Estuary, Wilmington, DE.
Labat, D., 2008. Wavelet analysis of the annual discharge records of the world's largest rivers. Adv. Water Resour. 31, 109–117.

Labat, D., 2010. Cross wavelet analyses of annual continental freshwater discharge and selected climate indices. J. Hydrol. 385, 269–278.
Latif, M., Barnett, T.P., 1996. Decadal climate variability over the North Pacific and North America: dynamics and predictability. J. Clim. 9, 2407–2423.
Latif, M., Keenlyside, N.S., 2008. El Niño/southern oscillation response to global warming. Proc. Natl. Acad. Sci. U. S. A. 106, 20578–20583.
Leathers, D.J., Yarnal, B., Palecki, M.A., 1991. The Pacific/North American teleconnection pattern and United States climate. Part I: regional temperature and precipitation associations. J. Clim. 4, 517–528.
Luksch, U., von Storch, H., 1992. Modeling the low-frequency sea surface temperature variability in the North Pacific. J. Clim. 5, 893–906.
Mantua, N.J., Hare, S.R., 2002. The Pacific decadal oscillation. J. Oceanogr. 58, 35–44.
Mantua, N.J., Hare, S.R., Zhang, Y., Wallace, J.M., Francis, R.C., 1997. A Pacific interdecadal climate oscillation and its impact on salmon production. Bull. Am. Meteorol. Soc. 76, 1069–1079.
Mattson, D.E., 1981. Statistics: Difficult Concepts, Understandable Explanations. Mosby, C.V., St. Louis, 482 pp.
Menne, M.J., Williams, C.N., Vose, R.S., 2009. The US historical climatology network monthly temperature data, version 2. Bull. Am. Meteorol. Soc. 90, 993–1007.
Miller, W.D., Kimmel, D.G., Harding, L.W.Jr., 2006. Predicting spring discharge of the Susquehanna River from a winter synoptic climatology for the eastern United States. Water Resour. Res. 42, http://dx.doi.org/10.1029/2005wr004270, W05414.
Najjar, R.G., 1999. The water balance of the Susquehanna River Basin and its response to climate change. J. Hydrol. 219, 7–19.
Najjar, R.G., Patterson, L., Graham, S., 2009. Climate simulations of major estuarine watersheds in the Mid-Atlantic region of the US. Clim. Change 95, 139–168.
Najjar, R.G., Pyke, C.R., Adams, M.B., Breitburg, D., Hershner, C., Kemp, M., Howarth, R., Mulholland, M.R., Paolisso, M., Secor, D., Sellner, K., Wardrop, D., Wood, R., 2010. Potential climate-change impacts on the Chesapeake Bay. Estuar. Coast. Shelf Sci. 86, 1–20.
Namias, J., 1966. Nature and possible causes of the Northeastern United States drought during 1962–65. Mon. Weather Rev. 94, 543–554.
Newman, M., Compo, G.P., Alexander, M.A., 2003. ENSO-forced variability of the Pacific decadal oscillation. J. Clim. 16, 3853–3857.
Ning, L., Mann, M.E., Crane, R., Wagener, T., Najjar, R.G., Singh, R., 2012. Probabilistic projections of anthropogenic climate change impacts on precipitation for the Mid-Atlantic region of the United States. J. Clim. 25, 5273–5291.
Notaro, M., Wang, W., Gong, W., 2006. Model and observational analysis of the Northeast U.S. regional climate and its relationship to the PNA and NAO patterns during early winter. Mon. Weather Rev. 134, 3479–3505.
Peters, K., Jakob, C., Davies, L., Khouider, B., Majda, A.J., 2013. Stochastic behavior of tropical convection in observations and a multicloud model. J. Atmos. Sci. 70, 3556–3575.
Philander, S.G.H., 1983. El Niño Southern Oscillation phenomena. Nature 302, 295–301.
Randall, D.A., Wood, R.A., Bony, S., Colman, R., Fichefet, T., Fyfe, J., Kattsov, V., Pitman, A., Shukla, J., Srinivasan Stouffer, J.R.J., Sumi, A., Taylor, K.E., 2007. Climate models and their evaluation. In: Solomon, S., Qin, D., Manning, M., Chen, Z., Marquis, M., Averyt, K.B., Tignor, M., Miller, H.L. (Eds.), Climate Change 2007: The Physical Science Basis. Contribution of Working Group I to the Fourth Assessment Report of the Intergovernmental Panel on Climate Change. Cambridge University Press, Cambridge, United Kingdom.
Seager, R., Pederson, N., Kushnir, Y., Nakamura, J., Jurburg, S., 2012. The 1960 drought and the subsequent shift to a wetter climate in the Catskill mountains region of the New York City watershed. J. Clim. 25, 6721–6742.
Seager, R., Kushnir, Y., Nakamura, J., Ting, M., Naik, N., 2010. Northern hemisphere winter snow anomalies: ENSO, NAO and the winter of 2009/10. Geophys. Res. Lett. 37, http://dx.doi.org/10.1029/2010gl043830, L14703.
Seager, R., Kushnir, Y., Herweijer, C., Naik, N., Velez, J., 2005. Modeling of tropical forcing of persistent droughts and pluvials over Western North America: 1856–2000. J. Clim. 18, 4065–4088.
Serreze, M.C., Clark, M.P., McGinnis, D.L., Robinson, D.A., 1998. Characteristics of snowfall over the eastern half of the United States and relationships with principal modes of low-frequency atmospheric variability. J. Clim. 11, 234–250.
Steinberg, N., Suszkowski, D.J., Clark, L., Way, J., 2004. Health of the harbor: the first comprehensive look at the state of the NY/NJ Harbor Estuary. In: A report to the NY/NJ Harbor Estuary Program. Tech. Rep. Hudson River Foundation, New York.
Thompson, D.W.J., Wallace, J.M., 1998. The Arctic oscillation signature in the wintertime geopotential height and temperature fields. Geophys. Res. Lett. 25, 1297–1300.
Thompson, D.W., Wallace, J.M., 2001. Regional climate impacts of the Northern Hemisphere annular mode. Science 293, 85–89.
Torrence, C., Compo, G.P., 1998. A practical guide to wavelet analysis. Bull. Am. Meteorol. Soc. 79, 61–78.
Trenberth, K.E., 1984. Signal versus noise in the Southern Oscillation. Mon. Weather Rev. 112, 326–332.
Trenberth, K.E., Hurrell, J.W., 1994. Decadal atmosphere—ocean variations in the Pacific. Clim. Dyn. 9, 303–319.
Trenberth, K.E., 1997. The definition of El Niño. Bull. Am. Meteorol. Soc. 78, 2771–2777.
Trenberth, K.E., Shea, D.J., 2005. Atlantic hurricanes and natural variability in 2005. Geophys. Res. Lett. 33, http://dx.doi.org/10.1029/2006gl026894, L12704.
USDA, 2000. Preparing for Drought in the 21st Century, A Report of the Drought Policy Commission, 48 pp.
Wallace, J.M., Gutzler, D.S., 1981. Teleconnections in the geopotential height field during the northern hemisphere winter. Mon. Weather Rev. 109, 784–812.
Whitney, M.M., 2010. A study on river discharge and salinity variability in the Middle Atlantic Bight and Long Island Sound. Cont. Shelf Res. 30, 305–318.
Xu, J., Long, W., Wiggert, J.D., Lanerolle, L.W., Brown, C.W., Murtugudde, R., Hood, R.R., 2012. Climate forcing and salinity variability in Chesapeake Bay, USA. Estuaries Coasts 35, 237–261.